Received: 14 May 2019 | Revised: 13 August 2019 | Accepted: 30 September 2019

DOI: 10.1002/cjce.23685

THE CANADIAN JOURNAL OF CHEMICAL ENGINEERING

Canadian Society for Chemical Engineering | For Our Future
Société canadienne de génie chimique | Pour notre avenir

ARTICLE

Local analysis of Marangoni effects during and after droplet formation

Jens S. Heine | **Hans-Jörg Bart**

Chair of Separation and Technology, TU Kaiserslautern, Kaiserslautern, Germany

Correspondence
Hans-Jörg Bart, Chair of Separation and Technology, TU Kaiserslautern, Gottlieb-Daimler-Straße 44, PO Box 3049, 67653 Kaiserslautern, Germany.
Email: bart@mv.uni-kl.de

Funding information
German Research Foundation

Abstract

The influence on the mass transfer in liquid-liquid extraction was investigated during droplet formation in a quiescent aqueous continuous phase for the two transition components, acetone and acetonitrile, in toluene. Both transition components have similar characteristics. However, an approximately eight times slower mass transfer of a droplet hanging on a capillary in relation to a rising droplet could be observed. The droplet formation time and the initial solute concentration are decisive for the mass transfer behaviour. A lower volumetric flow leads to slower droplet formation and a higher specific mass transfer area enhancing mass transfer, which is visualized via laser induced fluorescence (LIF). Additionally, as expected, higher initial solute concentrations promote Marangoni turbulences and thus mass transfer, which is measured via confocal Raman spectroscopy inside a fixed hanging droplet.

KEYWORDS

droplet formation, interfacial phenomena, Marangoni convection, mass transfer

1 | INTRODUCTION

Liquid-liquid extraction is used in numerous technical processes, for example, in the pharmaceutical, petrochemical, biochemical, or chemical industries. However, its fundamentals are still not fully understood. The process efficiency and product quality are substantially influenced by the specific interfacial area, which depends on the local droplet behaviour, such as droplet formation followed by rise, coalescence, and/or breakage.[1,2] For reliable modelling of extraction processes, droplet interactions and non-idealities, like Marangoni effects, have to be taken into account. In that respect mass transfer is influenced by Marangoni convection (interfacial flow) arising from surface tension gradients at high concentrations, which induce oscillations affecting droplet interactions. This already starts during droplet formation and experimental data from literature show that up to about 55%[3–6] or even up to 80%[7] of the mass transfer is already finished during droplet formation. Therefore, local and temporally highly resolved measurements are necessary to capture mass transfer induced by Marangoni convection during droplet formation.[8] Marangoni instabilities (strong interfacial flow) are observed[9] in systems where interfacial tension is sensitive to solute concentration gradients. The occurring tangential shear stress causes random fluid motion on the mobile interfacial surface, on the condition that the interfacial surface is not contaminated with surfactants, which could hinder interfacial motion.[10,11] In many cases, interfacial phenomena dominate essential properties, such as mass transfer rates or droplet rise velocities. It is evident that interfacial instabilities enhance mass transfer,[7,12] but an investigation of local mass transfer during droplet

formation has so far not been accomplished,[13] as only the overall behaviour has been reported.[7,14–18] Nowadays, there is also a big focus on the single droplet.[19–21]

The mass transfer behaviour is concentration dependent, whereby three different mass transfer regimes may exist starting from high to low concentration gradients (1-3).[22] The first two are only with high gradients and eddy diffusion and the last one is dominated by molecular diffusion.[12,22,23]

1. In the turbulent regime Marangoni convective mass transfer induces turbulences near the interface.[12,23]
2. In the eruptive regime at highest gradients, there is no simple relationship between mass transfer and the physical properties given in literature.[12,22,23]
3. In the diffusion regime the high gradients almost vanish and molecular diffusion prevails.[12,22,23]

Newman[24,25] is a standard reference for the calculation of the non-stationary mass transfer in spherical particles without internal circulation. The concentration profile is time and location dependent and described by a series development:

$$\mathbf{c}^* = -\frac{2\cdot R}{\pi\cdot r}\sum_{n=1}^{\infty}\frac{(-1)^n}{n}\cdot\sin\left(\frac{n\cdot\pi\cdot r}{R}\right)\cdot\exp\left(-(n\cdot\pi)^2\cdot Fo\right) \quad (1)$$

The time dependent average concentration in the droplet can be calculated by integrating Equation (1):

$$\mathbf{c}^* = \frac{6}{\pi^2}\sum_{n=1}^{\infty}\frac{1}{n^2}\cdot\exp\left(-(n\cdot\pi)^2\cdot Fo\right) \quad (2)$$

The approximate solution in Equation (3) with a maximum deviation of 0.1% is easier to apply[15,26–28] instead of the series development above.

$$Fo \le 0.15 : c^* = 1-6\cdot\sqrt{\frac{Fo}{\pi}}+3\cdot Fo \quad (3)$$

$$Fo \ge 0.15 : c^* = \frac{6}{\pi^2}\exp\left(-\pi^2\cdot Fo\right)$$

with:

$$Fo = \frac{4\cdot D_s\cdot t}{d^2} \quad (4)$$

An analytical extension of Newman's equations, for internal resistance, for droplets or bubbles with internal circulation was further developed by several authors.[15,29–32] It was assumed that the circulation is fast compared to diffusion and that the flow field in the droplet is similar to the laminar one even at a high circulation velocity. As a result, Equations (1)-(3) can further be used, if the Fourier number is extended with an effective diffusion coefficient as:

$$Fo_t = \frac{4\cdot D_t\cdot t}{d^2} \quad (5)$$

and:

$$D_t = T\cdot D_s \quad (6)$$

Here, the Fourier number $\mathbf{Fo_t}$ contains both the turbulent enhancement and the molecular diffusion coefficient. The turbulent constant, T, has to be identified in single droplet experiments. Since the inner turbulent vortexes have not been yet quantified, T is regarded as an adjustable parameter to describe experimental data.

2 | MATERIAL AND METHODS

The European Federation of Chemical Engineering (EFCE) standard test system,[33] toluene$_{(d)}$-acetone$_{(s)}$-water$_{(c)}$ (d = dispersed phase, s = solute, c = continuous phase), and the chemical system, toluene$_{(d)}$-acetonitrile$_{(s)}$-water$_{(c)}$, is used for all experiments. Toluene and acetonitrile (ACN) are with a purity >99.8% (Fischer Chemical) and acetone is with a purity of >99.9% (BDH Chemicals). The water for the experiments was purified through reserve osmosis (Hydrotec, Hydromos UO 50 W) and additional ion exchange (Hydrotec, Hydromos VE 17) yielding a conductivity of <0.5 $\mu S\cdot cm^{-1}$. Water and toluene were mutually saturated in order to avoid additional mass transfer.

2.1 | Droplet suction

The test cell (1) was made of glass, PTFE (polytetrafluoroethylene), and stainless steel. It is equipped with a heating/cooling jacket (see Figure 1) using a Julabo FP40-HC/6 thermostat at an operating temperature of 25°C. The droplet size control (3) on a stainless steel capillary (d_i = 1 mm, d_a = 1.2 mm) was via two high precision syringe pumps (9, 10) and the droplet from the funnel was sucked off (5) with a syringe pump (Cavro Centris Pump Base CG CM).

Through injecting a defined volume in a cross section (12) of organic phase (toluene, either with acetone or acetonitrile) being followed by water with

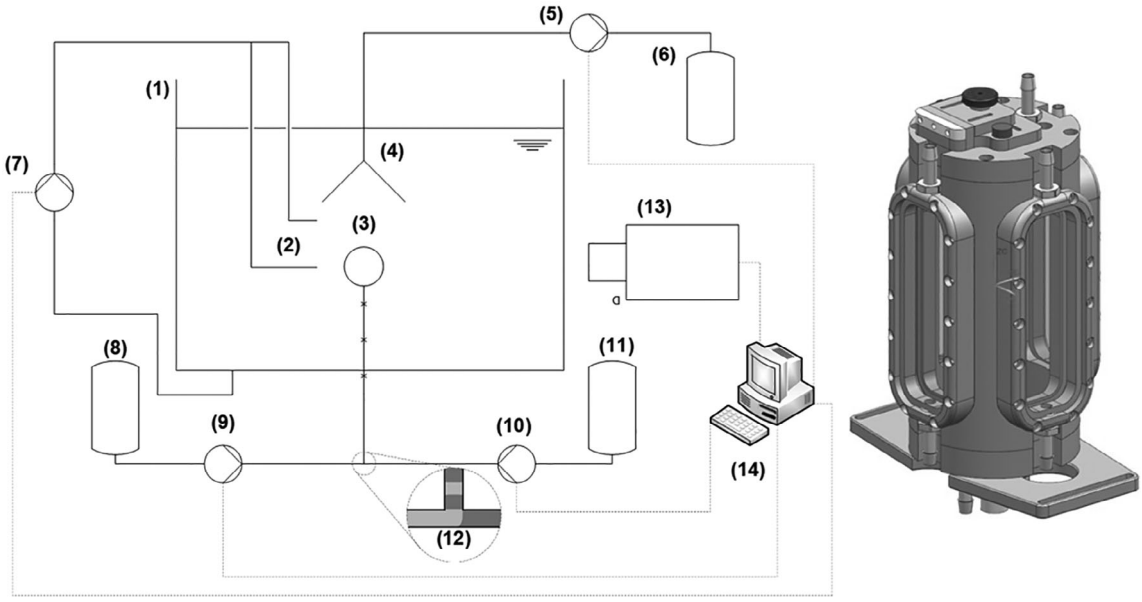

FIGURE 1 Experimental setup: (1) measurement cell, (2) flushing capillaries, (3) droplet at capillary, (4) droplet funnel, (5, 9, 10) precision syringe pump, (6) sample tank, (7) membrane pump, (8, 11) storage tank, (12) droplet generation, (13) high-speed camera, and (14) computer

acetone or acetonitrile, the droplet volume size can be adjusted precisely. There is no mass transfer in the feed line due to a mutual saturation of the phases in equilibrium. After the droplet formation (3), a short pulse of aqueous phase with the syringe pump (9) detaches the droplet from the capillary. This procedure is very sensitive to volume and velocity of the pulse so a gentle rise of the droplet will result. After the droplet rise, it is sucked off (4, 5); this procedure is repeated until sufficient volume (6) is available for gas chromatography (Agilent 6890 Series) analytics (three repeated measurements). For an exact measurement, the two flushing capillaries (2) destroy the occurring concentration zone over the total rising height by using a membrane pump (7), so that the same conditions exist for each measurement.

2.2 | Laser induced fluorescence (LIF)

For the LIF visualization, the tracer rhodamine 6G (0.2-20 μmol · L^{-1}) was added to the solute (acetone or ACN in toluene) in experiments with the mass transfer direction (d → c). The ultra-low fluorescence dye concentration does not influence physical properties, is well-soluble in water, acetone, and ACN and less soluble in toluene, and makes a LIF visualization possible.

Test cell (1) in Figure 2 is made of glass, PTFE (polytetrafluoroethylene), and stainless steel. It is equipped with a heating/cooling jacket using a Thermo Haake K10/DC30 thermostat to maintain an operating temperature of 25°C. The droplet size control (2) on a stainless steel capillary (d_i = 0.8 mm, d_a = 1 mm) was via a high precision syringe pump (8) (Hamilton PSD/3 mini). The laser beam (gem 532, Laser Quantum) (6) passes through the ultra-fast motorized laser beam shutter (standa) (5), which is triggered by the high-speed camera (IDT Os8) and subsequently widened to a flat beam by lenses (4) and directed into the measurement cell (1).

The image series (224 × 256 px) in this work was taken with 800 fps and therefore the ultra-fast motorized laser beam shutter (5) opened 800 times per second (possible up to 1000 opened-opened per second). Therefore, the laser (6) with a wavelength of 532 nm and 500 mW (possible range 50-2000 mW) always offers the same intensity on the droplets per image.

For calibration, a stock solution of the dispersed phase $c_{ACN,0}$ = 10 wt% acetonitrile +0.02 mmol · L^{-1} rhodamine 6G in toluene was prepared. For lower concentrations (up to 0.1 wt% solute concentration), it was diluted with toluene. For precise calibration any measured grey values were then assigned to the tracer concentration at different laser powers, initial concentrations, droplet sizes, and exposure times. As a result, there is a linear relationship between concentration and grey value (see Figure 3).

2.3 | Confocal Raman spectroscopy

A precision syringe pump (PSD/3-Mini module, Hamilton) is used to generate droplets of a well-defined volume in a newly designed measurement cell, as already described elsewhere.[34] It is made of stainless steel with the inner dimensions of 23 × 33 × 33 mm (H × W × Di) and a capillary height of 2 mm. The

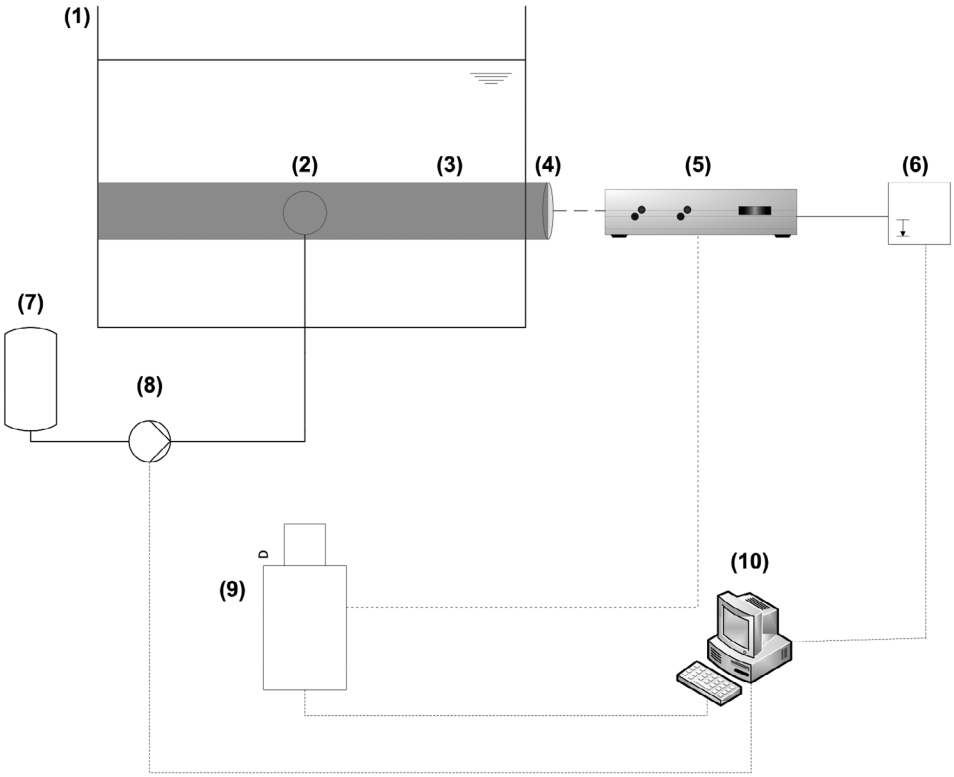

FIGURE 2 Experimental setup: (1) measurement cell, (2) droplet at capillary, (3) widened laser beam, (4) optics, (5) laser beam shutter, (6) laser, (7) storage tank, (8) precision syringe pump, (9) high-speed camera, and (10) computer

droplet is formed on a capillary, which has an inner diameter of 0.8 mm and an outer diameter of 1 mm. The measurement of the solute concentration inside the droplet is performed via a confocal Raman laser spectroscopy HR800 from Horiba (532 nm laser from Laser Quantum, type torus 532, software LabSpec6) in a volume of about 2 to 180 fL.

3 | RESULTS AND DISCUSSION

3.1 | Confocal Raman spectroscopy (fixed hanging droplet)

The solute concentration is measured in the exact middle of a hanging droplet (focused by microscopy), with an initial solute concentration of $c_{ACN,0}$ from 2.5 to 10 wt%, and a diameter of d = 2 mm (V = 4.2 μL) is depicted as dimensionless (Equation (7)) in Figure 4. The time-point 0 represents the concentration before droplet formation. All other concentrations are measured values.

$$c^* = \frac{c}{c_0} \tag{7}$$

The highest starting concentration ($c_{ACN,0}$ = 10 wt%) leads to the fastest mass transfer (T = 4). At lower concentrations the faster regimes (1 or 2) do not exist for the same amount of time as with higher concentrations, and, therefore, the mass transfer is slower and diffusion dominates. The initial mass transfer rate (gradient of the curve at t = 0) is, therefore, also much smaller at 2.5 wt%. The modified Newman[24,25] approach (see Equation (6)) described the experimental findings well.

However, if the concentration (c_0 = 10 wt%) and the droplet size (d = 2 mm) are kept constant and only the volumetric flow rate is changed (see Figures 5, 9, and 10), a significantly faster concentration decline is measured after the first seconds (see Figure 5) at low volumetric flow rates, compared to high ones. On the one hand, this

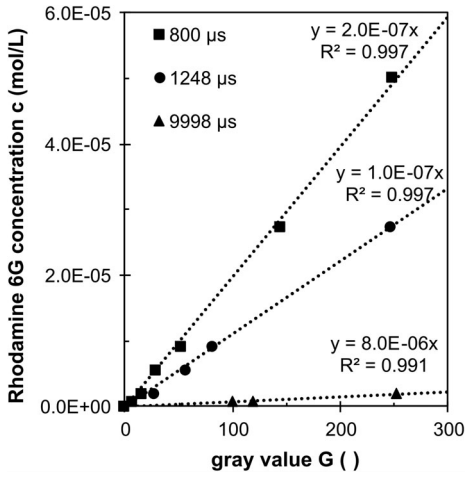

FIGURE 3 Grey value determination at constant laser power for three constant exposure times for different Rhodamine 6G concentrations

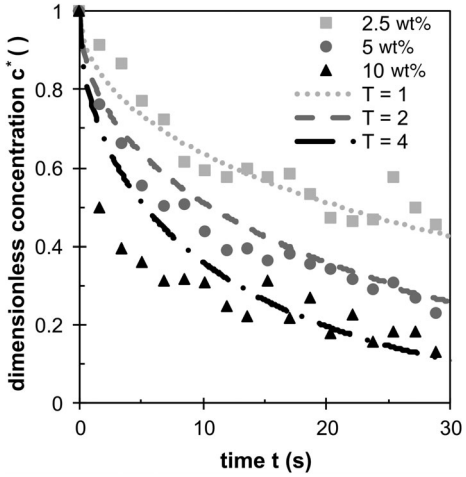

FIGURE 4 ACN concentration profiles: V = 4.2 µL, d = 2 mm, $\dot{V} = 50\,\mu L \cdot s^{-1}$ for different starting concentrations, $c_{ACN,0}$ = 2.5, 5, 10 wt%

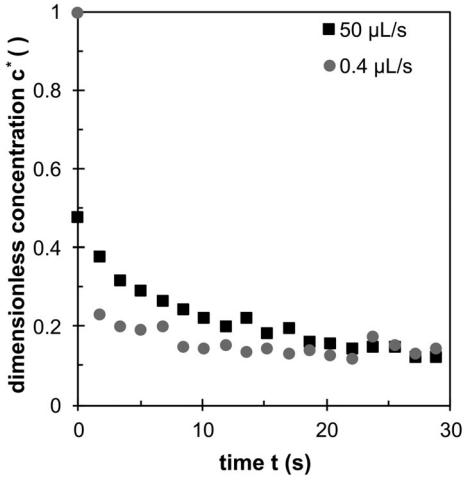

FIGURE 5 ACN concentration profiles in the middle of a droplet: V = 4.2 µL, d = 2 mm, $c_{ACN,0}$ 10 wt% for different volumetric flows, $\dot{V} = 50\,\mu L$ and $0.4\,\mu L \cdot s^{-1}$

is expected because the droplet has a better volume to surface ratio for a longer time with a lower volumetric flow and thus the mass transfer can take place more quickly[3,35] (see Figure 10). Thus, the mixing inside the droplet is more influenced by Marangoni convection and less by the volumetric flow rate.

On the other hand, the concentration profile inside the droplet during the first seconds is higher and more homogeneous mixed at a faster volumetric flow because the volumetric flow dominates the mixing inside the droplet (see Figures 9 and 5 (first seconds)). This results in a constant high concentration gradient, which leads to Marangoni convection immediately after and not during droplet formation, causing the droplet to wobble at the capillary. Thus, the solute around the droplet's circumference is better transported away and enhances mass

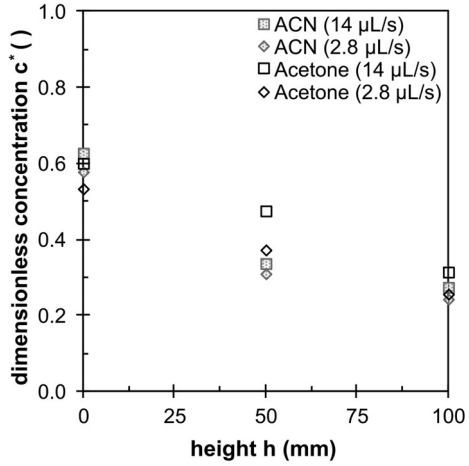

FIGURE 6 Acetone and ACN concentration profiles: V = 4.2 µL, d = 2 mm, $c_{ACN,0}$ = 10 wt% for different volumetric flows, $\dot{V}$ = 2.8 and $14\,\mu L \cdot s^{-1}$

transfer. However, approximately 20 seconds after droplet formation, both volumetric flows (see Figure 5) reveal a similar mass transfer behaviour when already 80% of the possible mass transfer is completed.

3.2 | Droplet suction (fixed hanging and moving droplet)

The overall concentration of the droplets can be determined by suctioning off the droplets at different rising heights respectively residence times. The difference between acetone and ACN were measured for two formation rates of a 2 mm droplet at different measurement heights with a starting concentration of c_0 = 10 wt% (see Figure 6).

It could be confirmed, that with a faster droplet formation, less mass transfer has taken place than with a slower formation rate for both solutes. These results are not unexpected, because the droplet has more time to release the solute when the droplet is formed more slowly[3,35] (see Figures 5 and 6). It is noteworthy that at a rising height of 0 mm in the time during droplet formation, approximately 40% of the mass transfer is already completed for both solutions and volumetric flows. However, at a rising height of 50 mm, approximately 65% and at a rising height of 100 mm approximately 73% of the mass transfer has already taken place. Thus, the droplet formation has a major influence on the mass transfer.

However, the comparison between ACN and acetone shows that ACN exhibits a slightly faster mass transfer. The marginal difference can be explained by a slightly larger ACN mixing gap as the EFCE test system under otherwise comparable physical properties.[33,36,37]

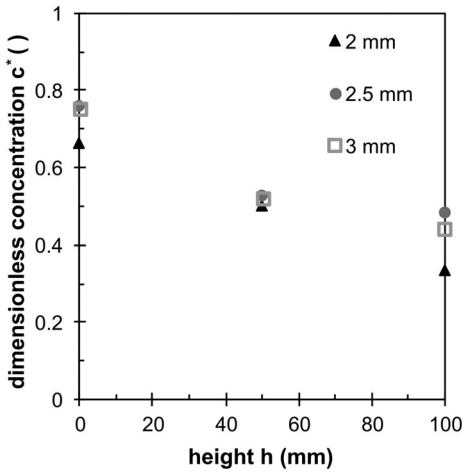

FIGURE 7 ACN concentration profiles: $c_{ACN,\,0} = 10$ wt%, $\dot{V} = 14\,\mu L \cdot s^{-1}$ for different droplet sizes

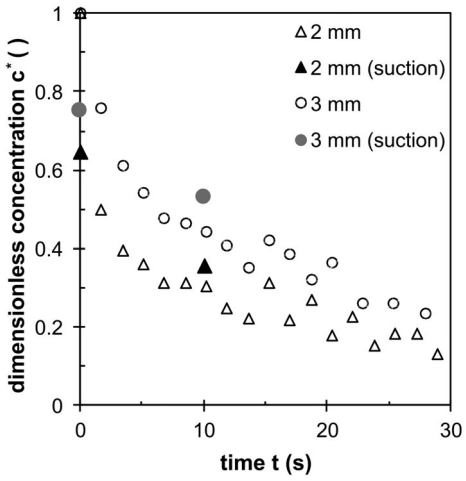

FIGURE 8 ACN concentration profiles: d = 2 and 3 mm, $c_{ACN,0} = 10$ wt%, $\dot{V} = 14\,\mu L \cdot s^{-1}$ (open symbols: Raman spectroscopy, full symbols: droplet suction)

At constant volumetric flow $\dot{\mathbf{V}} = 14\,\mu L \cdot s^{-1}$ and concentration $c_{ACN,0} = 10$ wt% with varied droplet size (see Figure 7), the mass transfer is faster with a higher surface to droplet volume ratio at 0 mm rising height. Under the same conditions as in Figure 7, the Raman measurement inside the droplet clearly shows a similar influence of the volume to surface ratio after droplet formation (see Figure 8). The decline of concentration of the larger (d = 3 mm) droplet is slower compared to the smaller (d = 2 mm) droplet. However, integral GC concentrations derived by droplet suction at 0 seconds and compared for a contact time after 10 seconds with a rising height of 0 mm correspond nicely with local Raman measurements (hanging droplet). In both cases a decline of about 65% of the initial concentration is measured for the smaller (d = 2 mm) droplet and about 50% for the larger (d = 3 mm) droplet. However, the solute transport is significantly influenced by the continuous phase hydrodynamics, as a fixed droplet has an approximately 8 times slower mass transfer compared to 100 mm rising droplet based on the contact time (see Figures 6 and 8). Here, the rising droplet has a contact time of approximately. 1.2 seconds compared to the hanging droplet, which has a contact time of 10 seconds. The droplet formation was identical in both cases.

3.3 | Laser induced fluorescence (droplet formation)

A sequence of droplet formation observed by the LIF system is shown in Figures 9 and 10 with the same starting concentration of $c_{ACN,0} = 10$ wt%, but at two different volumetric flow rates (2.5 and 10 $\mu L \cdot s^{-1}$). At a high volumetric flow rate in Figure 9, there are no internal turbulent vortexes during droplet formation and the liquid is quite evenly distributed. The white colour corresponds to high concentrations and the uprising feed flow causes slight swirls on the left and right side of the forming droplet (see Figure 9; 0.25 seconds), because of the small lower starting concentration on the top of the droplet (see Figure 9; 0.00 seconds). Thus, the volumetric flow rate of the feed dominates the mass transfer behaviour, which is rather low and looks similar to a pure diffusional regime, but is still convective inside the droplet. This corresponds to the Raman measured profiles (fixed hanging droplet) in Figure 5 after droplet formation and the droplet suction (rising droplet) in Figure 6.

At the reduced volumetric flow rate in Figure 10, the behaviour of the droplet formation changes decisively. Now the Marangoni mass transfer turbulences (grey zones, not white ones in Figure 10; 0.25 seconds) dominate over the impact of feed flow rate. A precise time comparison between the different volumetric flows shows that the mass transfer is already further advanced due to the much higher surface to volume ratio (higher specific mass transfer area) achieved at the lower volumetric flow. In the next 0.3 seconds, inner vortexes start on the left and right of the droplet at 0.35 seconds, quickly leading to a lower concentration. Additionally, these inner turbulent vortexes lead to a mixture of the concentration inside the droplet (0.45 and 0.55 seconds) and correspond to the first measurement points after droplet formation (see Figures 5 and 6).

4 | CONCLUSIONS AND OUTLOOK

The influence of the Marangoni effect on mass transfer at single droplets during and after droplet formation was

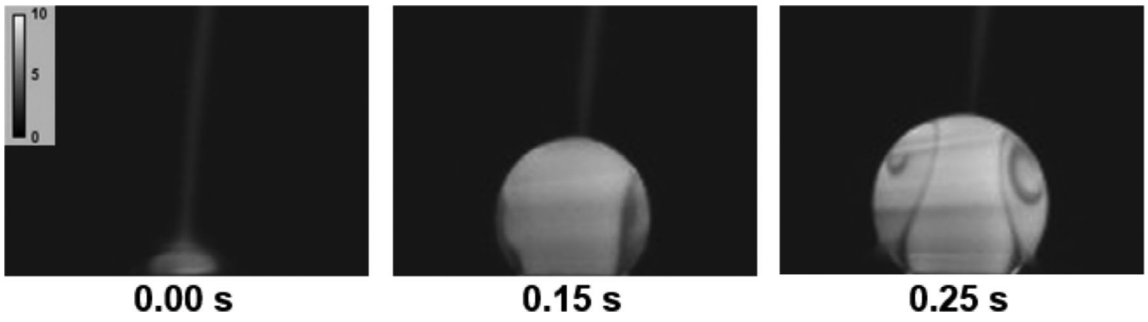

FIGURE 9 Droplet formation in different time steps of a toluene droplet (10 wt% acetone and 0.02 mmol · L^{-1} rhodamine 6G) with a formation rate of 10 μL · s^{-1}

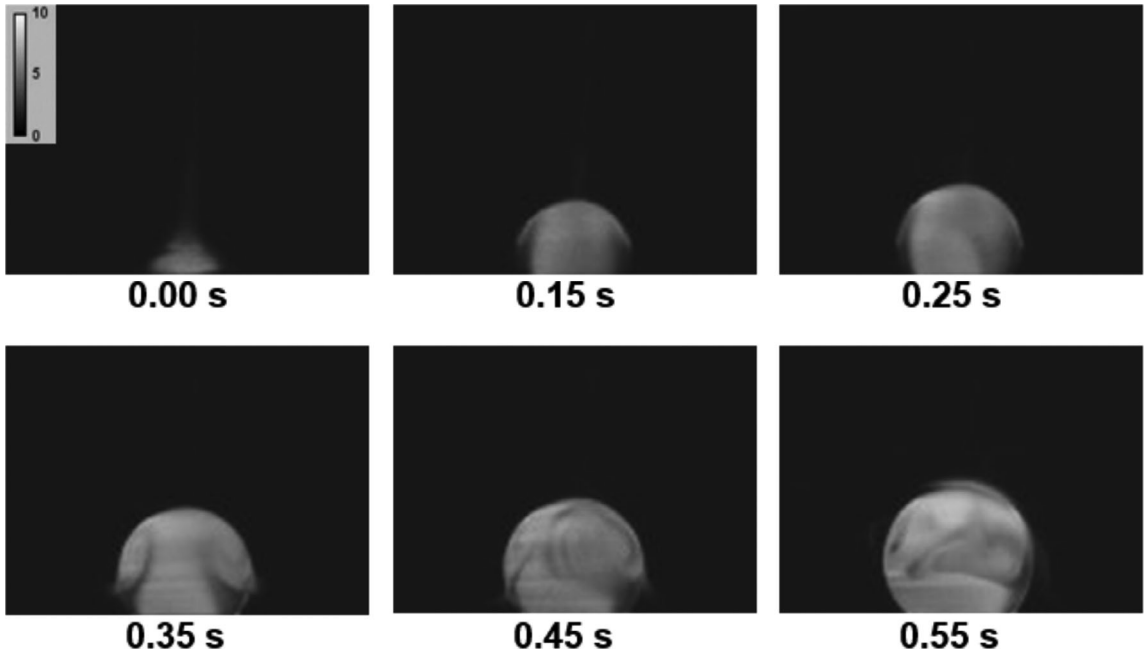

FIGURE 10 Droplet formation in different time steps of a toluene droplet (10 wt% acetone and 0.02 mmol · L^{-1} rhodamine 6G) with a formation rate of 2.5 μL · s^{-1}

studied with three independent methods: Raman measurement (fixed hanging droplet), droplet suction (hanging and rising droplet), and LIF (droplet formation). Confocal Raman spectroscopy allows high resolution measurements at distinct locations inside the droplet. In addition to this, the overall concentration of several droplets is determined by gas chromatography after droplet suction and collection. In general, a rapid decrease of the solute concentration during droplet formation and the first seconds after formation could be determined. In both cases (droplet suction and Raman microscopy), more than half of the mass transfer was completed after 10 seconds for a 2 mm hanging droplet. This is consistent with the results from literature, which report between 19% and 80% of the mass transfer occurs during droplet formation. However, at a rising height of 100 mm, almost the same decrease in concentration could be measured in relation to a 10 second hanging droplet. Thus, there is a big difference between a quiescent and a moving surrounding continuous phase around the droplet, which could explain the great differences in literature.

Nevertheless, the influence of the starting concentration inside the droplet was measured via Raman spectroscopy. It was determined that, at higher starting concentrations, the absolute mass transfer is faster and these differences could also be described with the modified Newman model. Furthermore, it is evident that the droplet size has an influence on the mass transfer, as a droplet at a low formation rate exhibits a larger surface to volume ratio, as well as the longer contact time, yielding a faster mass transfer.

The mass transfer enhancement by Marangoni convection during droplet formation could be visualized by LIF measurements for two different volumetric flows. It was recognized that the Marangoni turbulences inside the droplet are more strongly pronounced during droplet formation at a lower volumetric flow rate. This is due to the stronger concentration gradients, which are caused by the larger

surface to volume ratio. However, at higher volumetric flow rates, there is less mixing between different concentrations, which reduces the formation of strong concentration gradients. Thus, the mixing inside the droplet dominates at low volumetric flow rates by Marangoni convection and at higher volumetric flow rates more and more by the volumetric flow. The fact that the mass transfer is faster at lower formation rates could also be verified via Raman measurements on a hanging droplet after formation.

ACKNOWLEDGEMENT

The financial support provided by the German Research Foundation (DFG) is gratefully acknowledged.

NOMENCLATURE

c	concentration ($kg \cdot kg^{-1}$)
d	droplet diameter (m)
D	diffusion coefficient ($m^2 \cdot s^{-1}$)
Di	depth of the measuring cell (m)
Fo	Fourier number
G	grey value
H	height of the measuring cell (m)
n	count number
r	distance in radial direction (m)
R	droplet radius (m)
t	time (s)
T	turbulent enhancement factor
V	volume (m^3)
$\dot{V}$	flow rate ($m^3 \cdot s^{-1}$)
W	width of the measuring cell (m)
y	mass fraction of the solute ($kg \cdot kg^{-1}$)

Greek letters

ρ	density ($kg \cdot m^{-3}$)
σ	interfacial tension ($kg \cdot s^{-1}$)

Subscripts

*	dimensionless
0	initial
ACN	acetonitrile
c	continuous
d	disperse
s	solute
t	turbulent

REFERENCES

[1] F. Gebauer, J. Villwock, M. Kraume, H.-J. Bart, *Chem. Eng. Res. Des.* **2016**, *115*, 282.
[2] F. Gebauer, M. W. Hlawitschka, H.-J. Bart, *Chinese J. Chem. Eng.* **2016**, *24*, 249.
[3] T.-B. Liang, M. J. Slater, *Chem. Eng. Sci.* **1990**, *45*, 97.
[4] W. Licht, J. Conway, *Ind. Eng. Chem.* **1950**, *42*, 1151.
[5] W. Licht, W. Pansing, *Ind. Eng. Chem.* **1953**, *45*, 1885.
[6] F. B. West, P. A. Robinson, A. C. Morgenthaler Jr., T. R. Beck, D. K. McGregor, *Ind. Eng. Chem.* **1951**, *43*, 234.
[7] L. Steiner, G. Oezdemir, S. Hartland, *Ind. Eng. Chem. Res.* **1990**, *29*, 1313.
[8] C. Marangoni, *Annalen der Physik und Chemie* **1871**, *219*, 337.
[9] M. Wegener, A. R. Paschedag, *Int. J. Multiphas. Flow* **2011**, *37*, 76.
[10] D. Agble, M. A. Mendes-Tatsis, *Int. J. Heat Mass Tran.* **2000**, *43*, 1025.
[11] L. Mekasut, J. Molinier, H. Angelino, *Chem. Eng. Sci.* **1979**, *34*, 217.
[12] H. Sawistowski, *Chem.-Ing.-Tech.* **1973**, *45*, 1093.
[13] H. P. Khadamkar, M. A. Khanwale, S. S. Sawant, C. S. Mathpati, *Chem. Eng. Sci.* **2017**, *170*, 176.
[14] J. Wang, Z. Wang, P. Lu, C. Yang, Z.-S. Mao, *AIChE J.* **2011**, *57*, 2670.
[15] M. Henschke, A. Pfennig, *AIChE J.* **1999**, *45*, 2079.
[16] J. Chen, C. Yang, Z.-S. Mao, *Eur. Phys. J.-Spec. Top.* **2015**, *224*, 389.
[17] K. H. Javed, J. D. Thornton, T. J. Anderson, *AIChE J.* **1989**, *35*, 1125.
[18] J. B. Lewis, *Chem. Eng. Sci.* **1954**, *3*, 260.
[19] J. S. Heine, H.-J. Bart, *Chem. Eng. Technol.* **2019**, *42*, 1388.
[20] A. Javadi, M. Karbaschi, D. Bastani, J. K. Ferri, V. I. Kovalchuk, N. M. Kovalchuk, K. Javadi, R. Miller, *Colloid. Surface. A* **2014**, *441*, 846.
[21] A. Javadi, D. Bastani, M. Taeibi-Rahni, *AIChE J.* **2006**, *52*, 895.
[22] H. Sawistowski, B. R. James, *Chem.-Ing.-Tech.* **1963**, *35*, 175.
[23] W. K. Lewis, W. G. Whitman, *Ind. Eng. Chem.* **1924**, *16*, 1215.
[24] A. B. Newman, *T. Am. Inst. Chem. Eng.* **1931**, *27*, 203.
[25] A. B. Newman, *T. Am. Inst. Chem. Eng.* **1931**, *27*, 310.
[26] V. Alopaeus, *AIChE J.* **2000**, *46*, 2369.
[27] A. Mersmann, M. Kind, J. Stichlmair, *Thermische Verfahrenstechnik Grundlagen und Methoden*, Springer, Berlin **2005**.
[28] A. Mersmann, *Stoffübertragung*, Springer, Berlin **1986**.
[29] A. I. Johnson, A. E. Hamielec, *AIChE J.* **1960**, *6*, 145.
[30] A. E. Handlos, T. Baron, *AIChE J.* **1957**, *3*, 127.
[31] R. Kronig, J. C. Brink, *Appl. Sci. Res.* **1951**, *2*, 142.
[32] P. H. Calderbank, I. J. O. Korchinski, *Chem. Eng. Sci.* **1956**, *6*, 65.
[33] T. Misek, R. Berger, J. Schröter, European Federation of Chemical Engineering, Working Party on Distillation, Absorption, and Extraction, *Standard Test Systems for Liquid Extraction*, The Institution of Chemical Engineers, London, England **1985**.
[34] J. S. Heine, H.-J. Bart, *Chem.-Ing.-Tech.* **2017**, *89*, 1635.
[35] M. Wegener, *Ph.D. Thesis*, Technische Universität Berlin **2009**.
[36] C. V. S. R. Rao, K. V. Rao, A. Raviprasad, C. Chiranjivi, *J. Chem. Eng. Data* **1978**, *23*, 23.
[37] D. S. Rao, K. V. Rao, A. R. Prasad, C. Chiranjivi, *J. Chem. Eng. Data* **1979**, *24*, 241.

How to cite this article: Heine JS, Bart H-J. Local analysis of Marangoni effects during and after droplet formation. *Can J Chem Eng*. 2020;98: 1164–1171. https://doi.org/10.1002/cjce.23685